Optical method for measuring thermal accommodation coefficients using a whispering-gallery microresonator

D. Ganta,[1] E. B. Dale,[1] J. P. Rezac,[2] and A. T. Rosenberger[1,a)]
[1]*Department of Physics, Oklahoma State University, Stillwater, Oklahoma 74078-3072, USA*
[2]*L-3 Communications, 7500 Innovation Way, Mason, Ohio 45040-9699, USA*

(Received 4 May 2011; accepted 8 August 2011; published online 30 August 2011)

A novel optical method has been developed for the measurement of thermal accommodation coefficients in the temperature-jump regime. The temperature dependence of the resonant frequency of a fused-silica microresonator's whispering-gallery mode is used to measure the rate at which the microresonator comes into thermal equilibrium with the ambient gas. The thermal relaxation time is related to the thermal conductivity of the gas under some simplifying assumptions and measuring this time as a function of gas pressure determines the thermal accommodation coefficient. Using a low-power tunable diode laser of wavelength around 1570 nm to probe a microsphere's whispering-gallery mode through tapered-fiber coupling, we have measured the accommodation coefficients of air, helium, and nitrogen on fused silica at room temperature. In addition, by applying thin-film coatings to the microsphere's surface, we have demonstrated that accommodation coefficients can be measured for various gases on a wide range of modified surfaces using this method. [doi:10.1063/1.3631342]

I. INTRODUCTION

The rate of heat transfer between a solid surface and an ambient gas is characterized by the thermal accommodation coefficient (also known as energy accommodation coefficient), α. It is the ratio of the actual heat transfer rate to the rate that would be found if incident gas molecules were reflected from the surface in thermal equilibrium with it, so it is also the probability that a molecule colliding with the surface equilibrates with it.[1,2] Alternatively, the quantity $1-\alpha$ can be interpreted as the probability of an incident molecule reflecting specularly from the surface. These coefficients depend on the specific properties of the material-gas interface and are notoriously difficult to calculate from first principles, so experimental data are not just valuable, but essential. Accommodation coefficients have been determined using various experimental methods, most commonly involving some variation of the hot-wire cell comprising a heated metal filament coaxial with a metal cylinder.[1–3] Other measurement techniques include parallel-plate heat transfer,[4] molecular-beam surface scattering,[5] and, for nanoparticles, laser-induced incandescence.[6,7] Some modern applications for accommodation coefficients are in predicting the atmospheric drag on satellites,[1] calculating the heating of dust grains by gas collisions in interstellar space,[1] evaluating heat management in microelectronic or micromechanical systems,[4] and particle sizing.[6,7]

Whispering-gallery modes (WGMs) are high-quality-factor (high-Q) optical modes of dielectric microresonators. In a fused-silica microsphere (a few hundred μm in radius), light confined by total internal reflection and grazing the inner surface, propagating around the equator such that there are an integral number of wavelengths in the sphere's circumference, constitutes a WGM. A microsphere can be made by melting the end of an optical fiber, and low absorption and scattering losses provide the high Q. Light can be efficiently coupled into a WGM by optical tunneling from a tapered fiber tangent to the microsphere in its equatorial plane. A WGM can serve as a sensitive probe of its environment, through the environment's interaction with the WGM's evanescent component. For example, WGM resonances have been used for microcavity-enhanced laser or broadband absorption spectroscopy of molecules in the ambient gas or liquid.[8–10] Microresonators have also been used as environmental probes that make use of the temperature sensitivity of WGM resonance frequencies.[11–16]

In the work reported here, heat transfer between a bare or thin-film-coated fused-silica microsphere and the ambient gas is studied by observing temperature-dependent shifts in WGM frequencies over a range of gas pressures. The microsphere is heated by focusing an external laser beam onto it; upon turnoff of the heating beam, the microsphere relaxes back to room temperature. From its relaxation rate, observed via the frequency shift of WGMs probed by a tunable diode laser operating at a wavelength of about 1570 nm, we can calculate the thermal conductivity of the surrounding gas (air, helium, or nitrogen). The gas's thermal conductivity thus determined as a function of pressure in the temperature-jump regime[1–3] gives us the thermal accommodation coefficient of the gas on the bare or coated surface. This novel optical method is employed at room temperature but any temperature below the softening point of fused silica (~1900 K) could be used.[15] Advantages of this method include the following: (i) because of the milliKelvin sensitivity of WGM shifts, the microsphere needs to be heated only about 1 K above the ambient gas temperature, and this small temperature difference (at least one order of magnitude smaller than in most other methods) makes the analysis given in Sec. II an even better

a)Electronic mail: atr@okstate.edu.

approximation;[1] (ii) various gases can be used; (iii) the surface can be treated (e.g., silanized) or coated with a thin film, provided only that the film is thin compared to the wavelength and that the Q of the WGM is not severely degraded; and (iv) the wavelength range can be chosen to minimize absorption in the gas and/or maximize the cavity Q. The results presented here represent a significant advance over our previously reported work.[16]

II. ANALYSIS

The theoretical treatment used for analysis of thermal relaxation measurements in the temperature-jump regime incorporates several simplifying, but well-justified, assumptions. First, the temperature throughout the body of the microsphere is uniform at all times because its internal thermal relaxation is very fast compared to the rate of heat transfer to the ambient gas;[17] this is discussed further at the end of this section. Second, as the microsphere cools, heat loss occurs only through conduction by the surrounding gas and by radiation; since the microsphere is so small, convection is negligible (see comments at the end of this section),[18] and because its mounting stems are so thin, their thermal conduction is negligible, as demonstrated below in Sec. IV. Third, T, defined to be the deviation of the microsphere's temperature T_s above room temperature T_R, satisfies $T = T_s - T_R \ll T_R$ (typically, $T \sim 1$ K and $T_R \sim 298$ K), and so the temperature dependences of the thermal conductivity and specific heats of the gas may be neglected. The fourth assumption is that the actual prolate microspheroid is a perfect sphere with some effective radius a; this is discussed in more detail later in this section and again in Sec. IV.

The total rate of heat loss from the microsphere thus has two parts, a component due to conduction through the gas and a radiative component:

$$\dot{Q} = \dot{Q}_c + \dot{Q}_r. \tag{1}$$

The radiative heat loss rate is given by

$$\begin{aligned}\dot{Q}_r &= 4\pi a^2 \varepsilon\sigma \left(T_s^4 - T_R^4\right) \cong 16\pi a^2 \varepsilon\sigma T_R^3 \left(T_s - T_R\right) \\ &= 16\pi a^2 \varepsilon\sigma T_R^3 T,\end{aligned} \tag{2}$$

where $\epsilon = 0.87$ is the emissivity of fused silica, and σ is the Stefan-Boltzmann constant. Assume for now that a is the measured radius of a perfectly spherical microresonator. The conductive heat loss rate is given by the Fourier law, which for heat transport outward through a spherical surface of radius r reads

$$\dot{Q}_c = -4\pi r^2 k \frac{dT_g}{dr}, \tag{3}$$

where k is the thermal conductivity of the gas, and T_g is its local temperature. The remaining analysis is specific to the temperature-jump (or slip-flow) regime. Take the Knudsen number, Kn, to be given by the ratio of the molecular mean free path to the microsphere radius. For $Kn < 0.01$, the system is in the continuum regime, and for $Kn > 10$ it is in the free-molecular-flow regime. Midway between those limits, the temperature-jump model applies. The majority of our relevant experimental data lie in the range $0.05 < Kn < 0.3$, so our system is in the temperature-jump regime.

In the temperature-jump regime, there is an apparent temperature discontinuity at the solid-gas interface that increases as the gas pressure is decreased. Approaching the surface of the sphere, the gas temperature rises according to Eq. (3) until, very near the surface, it increases more rapidly to equal T_s at $r = a$; without this temperature jump, the effective gas temperature at the surface would be T_e. Extrapolating the gas temperature gradient of Eq. (3) to the sphere's surface, the temperature-jump distance g is defined by

$$T_s = T_e - g\left(\frac{dT_g}{dr}\right)_a = T_e + g\frac{\dot{Q}_c}{4\pi a^2 k}. \tag{4}$$

The heat flow is assumed to be from the surface of the microsphere to a distant concentric spherical surface at T_R, where there is another temperature jump that becomes negligible as the radius of this imaginary surface becomes infinite. T_e can be found by integrating Eq. (3):

$$\frac{\dot{Q}_c}{4\pi}\int_a^\infty \frac{dr}{r^2} = -\int_{T_e}^{T_R} dT_g, \tag{5}$$

which gives

$$T_e = T_R + \frac{\dot{Q}_c}{4\pi a k}, \tag{6}$$

and so substituting into Eq. (4) gives

$$\dot{Q}_c = \frac{4\pi a k}{1 + \frac{g}{a}} T. \tag{7}$$

Thus, the total heat flow rate can be written as

$$\dot{Q} = \left(4\pi a k_{\text{gas}} + 16\pi a^2 \varepsilon\sigma T_R^3\right) T, \tag{8}$$

and the microsphere-room temperature difference decays as

$$\frac{dT}{dt} = -\frac{\dot{Q}}{mc} = -\frac{1}{mc}\left(4\pi a k_{\text{gas}} + 16\pi a^2 \varepsilon\sigma T_R^3\right) T = -\frac{1}{\tau}T, \tag{9}$$

where m is the mass of the microsphere (found from its volume, taking the density of fused silica to be $\rho = 2.20 \times 10^3$ kg m^{-3}), $c = 741$ J kg^{-1} K^{-1} is the specific heat of fused silica, and τ is the thermal relaxation time. In Eqs. (8) and (9), the thermal conductivity of the ambient gas is given by

$$k_{\text{gas}}(p) = \frac{k}{1 + \frac{g}{a}} = \frac{k_{\text{atm}}}{1 + \left[\frac{(2-\alpha)}{\alpha}\right]\frac{k_{\text{atm}}\sqrt{2\pi RT_R}}{(c_p + c_v)pa}}, \tag{10}$$

where the continuum limit of the gas's thermal conductivity is taken to be its value at atmospheric pressure ($k = k_{\text{atm}}$), R is the gas constant per unit mass of gas, c_p and c_v are the specific heats of the gas at constant pressure and volume, respectively, and p is the gas pressure. From the definitions of the thermal accommodation coefficient α and the temperature-jump distance g, the standard relation between them that is incorporated into Eq. (10) may be derived.[1,3,6,19] This equation then shows how the measured k_{gas} decreases with decreasing pressure in the temperature-jump regime, as the mean free path becomes comparable to the radius of the microsphere. Therefore, measuring the thermal relaxation time τ as a function of

TABLE I. Properties of the various ambient gases used in this work.

Gas	k_{atm} (W/m K)	R (kJ/kg K)	c_p (kJ/kg K)	c_v (kJ/kg K)
Air	0.0259	0.287	1.01	0.718
Helium	0.155	2.077	5.19	3.12
Nitrogen	0.0259	0.297	1.04	0.743

pressure determines experimental values of $k_{gas}(p)$ according to Eq. (9), and fitting those data to Eq. (10) gives the thermal accommodation coefficient α.

Since the microresonators used in this work are not perfectly spherical, but approximately prolate spheroids, the model fitting proceeds in a different manner. Equation (10) is substituted into Eq. (9) to produce a model for $1/\tau$ vs. p that is fit to the data found from the measured thermal relaxation times τ and pressures p to determine the effective radius a and the accommodation coefficient α and their uncertainties. A two-parameter nonlinear least-squares fit is used, with effective-variance weighting[20] to take account of uncertainties in p as well as in $1/\tau$. Experimental values of $k_{gas}(p)$ are then found using the following relation derived from Eq. (9):

$$k_{gas} = \frac{\rho c a^2}{3\tau} - 4a\varepsilon\sigma T_R^3, \tag{11}$$

and plotted with the model curve from Eq. (10) for comparison. Values of the particular gas parameters used here are given in Table I.

Some further justification of our first two assumptions will now be given. A uniform temperature distribution within the microsphere can be assumed because its Biot number (Bi) is small compared to 1.[21] For a sphere, the Biot number is given by a particularly simple expression:

$$Bi = \frac{ha}{k_{fs}} = \frac{k_{gas}}{k_{fs}}, \tag{12}$$

where h is the surface heat transfer rate, and k_{fs} = 1.38 W/m K is the thermal conductivity of fused silica. The maximum value of the Biot number is thus k_{atm}/k_{fs}, and in our experiments its range is $0.02 < Bi_{max} < 0.10$. Convection can be neglected because the system's Grashof number (Gr) is less than 7×10^{-3} in all cases.[22] Since the Prandtl number of the gases used is approximately $Pr = 0.7$, this means that the Rayleigh number, $Ra = GrPr$, is never larger than 5×10^{-3}, and thus heat loss due to convection makes a negligibly small contribution to the total.

III. EXPERIMENTAL SETUP AND METHOD

The thermal relaxation time τ at a selected pressure is found by measuring the time dependence of the WGM frequency shift as the heated microsphere cools back to room temperature, after the focused laser beam that heats it is turned off. The microsphere is mounted, polar axis (stem) vertical, inside the cylindrical vacuum chamber shown in the experimental setup illustrated in Fig. 1. The vacuum chamber is 20 cm in diameter and 11 cm high and has a transparent top plate and side windows for viewing. Using a mechanical pump, the gas pressure in the chamber can be reduced from atmospheric

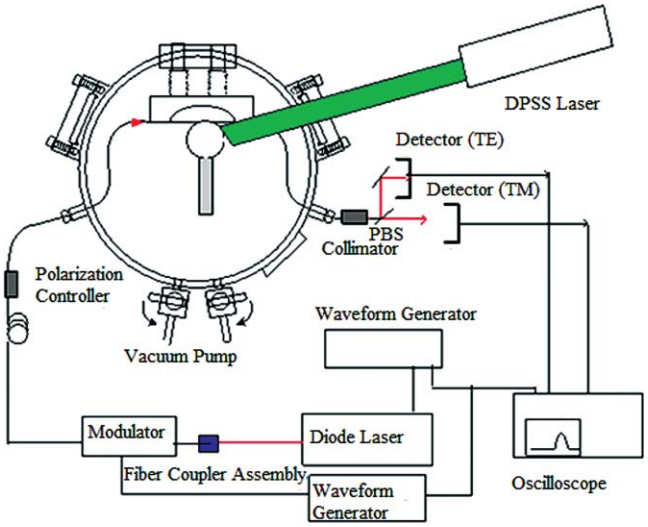

FIG. 1. Experimental setup. A fused-silica microsphere is mounted inside a vacuum chamber in which the ambient gas and pressure are controlled. After the microsphere is heated by a diode-pumped solid state (DPSS) laser, its WGM frequency spectrum is probed by light from a frequency-scanned cw diode laser that is launched into a bi-tapered fiber to excite TE or TM modes. A polarizing beamsplitter (PBS) separates throughput of the two polarizations.

pressure (760 Torr; 1 Torr = 133.3 Pa) to about 1 mTorr. The other valve controls the intake of the gas being used, either room air or high purity helium or nitrogen. Not shown in Fig. 1 are the two capacitance manometers (MKS Baratron model 122B, 10 and 1000 Torr ranges) used for pressure measurement. The manometers are calibrated to atmospheric pressure, to zero pressure (1 mTorr is below their resolution limit), to each other, and to a thermocouple gauge on the pump station.

Light from a cw tunable diode laser (New Focus model 6328, linewidth < 300 kHz) is fiber-coupled into a lithium niobate Mach-Zehnder amplitude modulator, from which it exits into a single-mode optical fiber that passes through a polarization controller before being fed into the vacuum chamber, where its adiabatic bitapered region is brought into contact with the microsphere for evanescent excitation of WGMs. This coupling fiber was tapered to a diameter of 2–3 μm using the flame brush technique; its position is controlled by 3D stages located outside the chamber. The polarization controller seen in Fig. 1 is adjusted to ensure that WGMs of a single polarization (transverse electric, TE, is vertical; transverse magnetic, TM, is horizontal) are excited, and after the fiber is fed out of the chamber the throughput is detected by one of two Newport 818-IR detectors, depending on polarization. The modulator is normally off, but can be turned on to provide a square-wave intensity modulation; the throughput response to the square-wave input tells us whether a WGM is undercoupled or overcoupled (intrinsic or coupling loss dominant, respectively) without changing the geometry of the system. That information is not needed for the results presented here. The 532-nm heating beam of about 1–2 W comes from a frequency-doubled Nd:YVO_4 diode-pumped solid state (DPSS) laser (Spectra-Physics Millennia) and is focused through a side window onto the microsphere as shown in Fig. 1.

As the diode laser is scanned in frequency, the position of each WGM is marked by a Lorentzian dip in the throughput power. In these experiments, the external beam heats the microsphere to ∼1 K above room temperature and is then turned off. At wavelengths around 1570 nm, the WGM resonance frequency is expected to redshift by ∼1.6 GHz for each Kelvin increase in temperature. This shift is primarily due to the temperature-dependent change in refractive index,[23] augmented by the effect of thermal expansion. Measurements performed under conditions of controlled heating of the entire vacuum chamber yield an average linear redshift of 1.60 GHz/K. Displacement of a WGMs throughput dip from one scan trace to the next is analyzed to find the relaxation time constant as the microsphere returns to room temperature. This is done over a wide range of pressures from 30 mTorr to 760 Torr. Fitting the inverse thermal relaxation time vs. pressure data determines the effective radius and thermal accommodation coefficient as discussed earlier. A typical WGM in a bare or coated microsphere will have a Q of about 3×10^7 (including coupling losses) and thus its throughput dip will have a full width at half-maximum depth of about 6 MHz, resulting in a temperature-change measurement sensitivity of about 1 mK. For some surface-treated or coated microspheres, Q tends to be about an order of magnitude lower, changing the temperature resolution to about 10 mK. Therefore, a maximum T of 1 K or so is more than adequate for determination of α.

The diode laser is scanned up and down in frequency by a triangle wave; the scan rate had previously been calibrated by reference to fiber resonator transmission fringes. Ideally, the scan would be linear in time and have the same rate in both directions, but in practice there is a slight residual scan nonlinearity due to hysteresis in the piezoelectric actuator that scans the diode laser's frequency. Thus, mode-shift measurements from the two scan directions are averaged to reduce error.

IV. RESULTS

A. Single-stem microspheres

In these initial experiments, the accommodation coefficient of air on bare fused silica was found, using microspheres formed by melting the end of a tapered fiber. Data for two such microspheres, along with the fitted Eq. (10), are presented in Fig. 2.

The two microspheres represented in Fig. 2 were slightly prolate; the larger one had an effective radius, determined from the least-squares fit of $1/\tau$ vs. p described in Sec. II above, of $a = 179 \pm 1$ μm and a stem diameter of 10 μm; the smaller one had an effective radius of $a = 78 \pm 1$ μm and a stem diameter of 20 μm. The horizontal error bars on the data points reflect the 20-mTorr pressure measurement precision; the vertical error bars reflect the uncertainties in the measured thermal relaxation times, combined via standard error propagation with the uncertainty in the fitted effective radius. The accommodation coefficient of air on fused silica found by fitting the $1/\tau$ vs. p results from the larger sphere, $\alpha = 0.770 \pm 0.012$, is consistent with literature values.[1] However, in this case heat loss by stem conduction is not negligible for the smaller sphere, so the fit gives an anomalously large α value (0.997 ± 0.012).

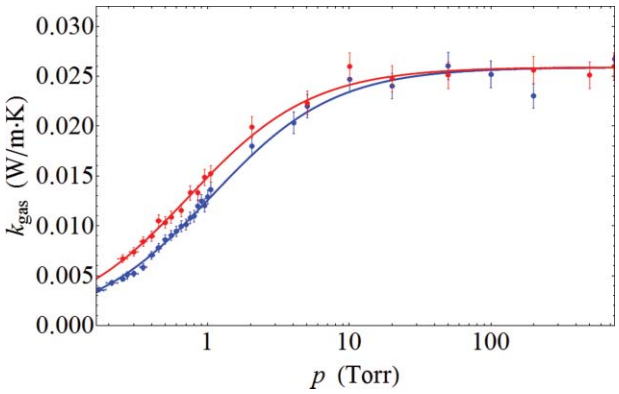

FIG. 2. Thermal conductivity of air vs. pressure, measured using two bare single-stem microspheres of different effective radii a and different stem diameters. The lines are the fitted Eq. (10); the fit gives $\alpha = 0.770 \pm 0.012$ for the larger sphere ($a = 179 \pm 1\mu$m, red, upper curve) and $\alpha = 0.997 \pm 0.012$ for the smaller sphere ($a = 78 \pm 1\mu$m, blue, lower curve).

To see how thin the stem must be for its heat conduction loss to be negligible, consider adding a term representing its heat conduction to Eq. (8):

$$\dot{Q} = \left(\frac{4\pi a k_{\text{atm}}}{1 + \frac{g}{a}} + 16\pi a^2 \varepsilon \sigma T_R^3 + \frac{\pi b^2 k_{fs}}{L_{\text{stem}}} \right) T, \tag{13}$$

where b is the radius of the stem, and L_{stem} is its length (distance from microsphere to heat sink at room temperature). Evaluating the three terms in Eq. (13) for the small sphere at low air pressure ($g/a = 15$), with $a = 78$ μm, $k_{\text{atm}} = 0.0259$ W/m K, $T_R = 298$ K, $b = 10$ μm, $k_{fs} = 1.38$ W/m K, $L_{\text{stem}} = 2$ mm, and $T = 1$ K gives 1.5, 0.40, and 0.22 μW for the air conduction, radiation, and stem conduction heat loss rates, respectively. Clearly, stem conduction is not negligible. For the larger sphere, the three terms are 3.5, 2.1, and 0.05 μW, so stem conduction may be small enough to be negligible. In order to be able to definitively neglect its heat conduction, the microsphere's stem needs to be quite thin. Unfortunately, a very thin stem makes rigid mounting of the microsphere difficult; this problem was overcome by fabricating microspheres with two stems. With two stems of radius 1.8 μm and 4 mm length each, and a microsphere radius of 320 μm, the three terms are 6.0, 6.4, and 0.007 μW, respectively, and we can be confident that stem conduction may be neglected.

B. Double-stem microspheres

In this section, we first discuss some improvements to the method and then present experimental results, for bare and coated fused-silica microspheres in three ambient gases. The experiments described above and our previously reported results[16] have a lot of data scatter. This is because the probe power from the tunable diode laser was high enough to cause slight heating of the sphere; the data scatter is due to fluctuations in the temperature of the sphere owing to differing heating efficiencies for different resonant WGMs excited during a frequency scan. To avoid this problem, the experiments described below are run at very low probe powers (<1 μW), scaled down from the 0.2–0.4 mW used earlier.

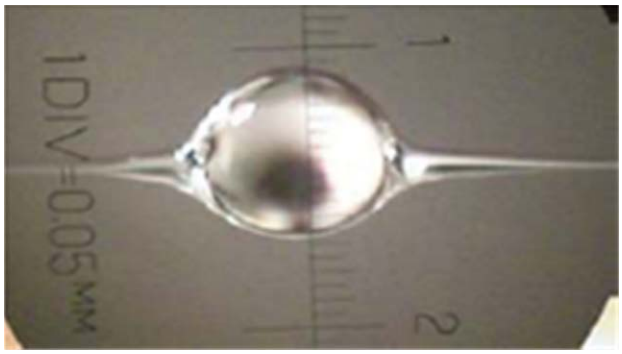

FIG. 3. Photograph of a bare fused-silica microsphere with two thin stems. This one has an effective radius in air, as defined in the text, of 290 ± 1 μm.

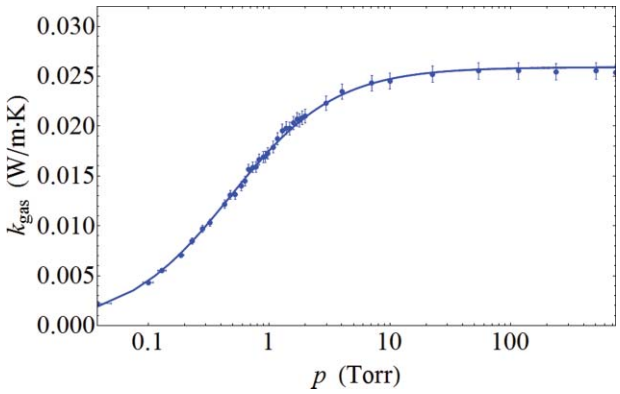

FIG. 4. Thermal conductivity of air vs. pressure, measured using a bare microsphere. The line is the fitted Eq. (10); the fit gives effective radius $a = 290 \pm 1$ μm, and thermal accommodation coefficient $\alpha = 0.745 \pm 0.006$.

To minimize heat loss by stem conduction and allow for rigid mounting, microresonators were fabricated from optical fiber in such a way as to have very thin stems at both poles; an example is shown in Fig. 3. The two stems can be made very thin, tapering to diameters of only about 3 μm. These microresonators are made by mounting two stripped and cleaned fibers into the two uniaxial translation stages of our taper puller so that they meet end-to-end and then gently heating their junction with a hydrogen-oxygen torch while pushing them together. Stronger heating then forms a microsphere; subsequently, each stem is flame-brush heated and stretched by pulling it away from the resonator with its translation stage until the stem tapers to the desired diameter. The two stems are then epoxied to a rigid mount before being removed from the translation stages.

These two-stem microresonators are more or less highly prolate spheroids but are treated as spheres with an effective radius found from the fit of the model to the $1/\tau$ vs. p data as described in Sec. II. In all cases, it was found that this effective radius is just slightly larger than the minor radius of the spheroid, perhaps because of the effect of tapering at the poles (Fig. 3). Alternatively, for a spheroid, its major and minor radii could be combined to give expressions for the effective radius of a sphere with the same volume, for the effective radius of a sphere with the same surface area, and for the global average of the local mean radius of curvature.[24] Each of these effective radii would appear at different points in the derivation of Eqs. (9) and (10) for a prolate spheroid. These modified equations could be used for analyzing the data from perfect spheroidal microresonators by using the measured minor and major radii and doing a one-parameter fit to find the accommodation coefficient. However, our resonators are not perfect spheroids because of the tapering at their poles. This tapering introduces an uncertainty of about 15% in determining the major radius, negating any advantage of using this three-effective-radius model, so the simpler method was used, treating the microresonator as a sphere of effective radius a, found along with the accommodation coefficient by a two-parameter fit.

In this work, the ambient gas will interact with the surface of a fused-silica microsphere that has been prepared in one of several ways. Different surfaces are obtained by using: (i) bare spheres; (ii) spheres coated with a 1-nm-thick film of the polyelectrolyte polydimethyldiallylammonium chloride (PDDA); and (iii) spheres with their surfaces silanized with aminosilane to provide a surface layer of amine groups, limiting the adsorption of water from the ambient gas. The PDDA coating was applied by immersing the microsphere for an hour in a 0.5% aqueous solution,[25] followed by rinsing in deionized water to remove any unbonded PDDA. After coating, the cavity's quality factor was compared to the quality factor before coating and no appreciable change was observed.

Silanization with different silane compounds can be done to provide a treated surface ranging from hydrophobic to polar.[26,27] Silanization of the microsphere with aminosilane, as done here, makes the surface more hydrophobic. During the silanization reaction, –Cl, $–OCH_3$, and $–OCH_2CH_3$ groups are converted to –OH groups and these –OH groups react with other –OH groups on the surface of the silica microsphere. These reactive alkoxy groups crosslink with the silica surface to different extents. We dipped the bare microsphere in a 5% solution of 3-aminopropyltriethoxysilane in a 95% ethanol–5% water mix for 30 min, then subsequently rinsed it with ethanol and dried it in a 120 °C oven.[10] The Q of the microresonator after silanization is usually reduced by somewhat more than an order of magnitude.

Results using the two-stem microspheres in air are given in Figs. 4–6, where, as in Fig. 2, the effective radius and accommodation coefficient are determined from the

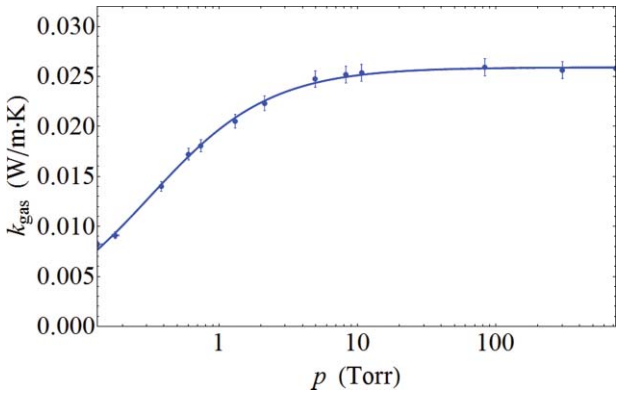

FIG. 5. Thermal conductivity of air vs. pressure, measured using a PDDA-coated microsphere. The line is the fitted Eq. (10); the fit gives effective radius $a = 391 \pm 1$ μm, and thermal accommodation coefficient $\alpha = 0.802 \pm 0.011$.

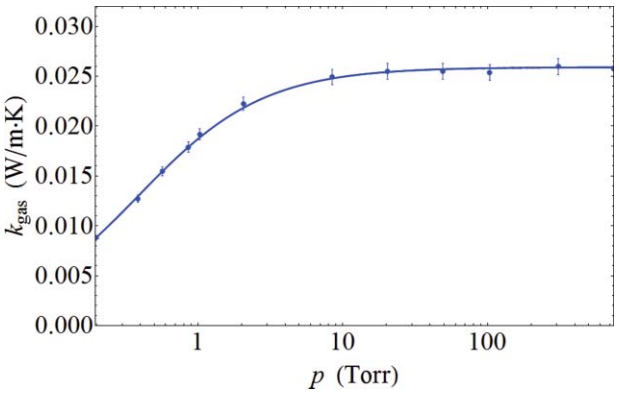

FIG. 6. Thermal conductivity of air vs. pressure, measured using a microsphere silanized with aminosilane. The line is the fitted Eq. (10); the fit gives effective radius $a = 344 \pm 1$ μm, and thermal accommodation coefficient $\alpha = 0.767 \pm 0.008$.

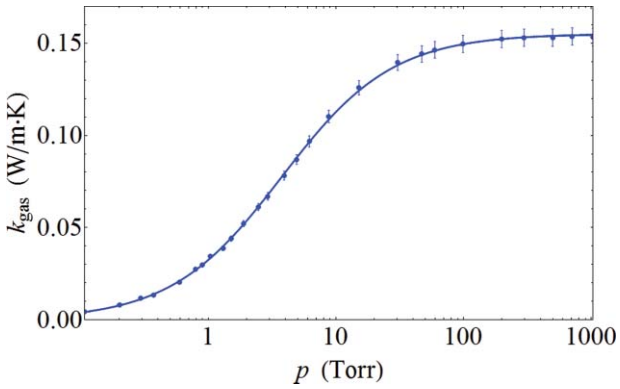

FIG. 7. Thermal conductivity of helium vs. pressure, measured using a bare microsphere. The line is the fitted Eq. (10); the fit gives effective radius $a = 299 \pm 1$ μm, and thermal accommodation coefficient $\alpha = 0.394 \pm 0.003$.

least-squares fit of $1/\tau$ vs. p data as described in Sec. II above, the horizontal error bars on the data points reflect the 10-mTorr pressure measurement precision, and the vertical error bars reflect the uncertainties in the measured thermal relaxation times, combined with the uncertainty in the fitted effective radius. The results in Fig. 4 give α of air on fused silica to be 0.745 ± 0.006. The α value for air on PDDA was found to be 0.802 ± 0.011 (Fig. 5). For air on silanized fused silica, α was found to be 0.767 ± 0.008 from Fig. 6. The higher α for air on PDDA reflects the porosity of the coating and perhaps also the somewhat increased surface charge (of opposite sign from that of bare silica). These and all other results for accommodation coefficients are summarized in Table II at the end of this section.

The α value for helium on fused silica is found to be 0.394 ± 0.003, from the fit to the data shown in Fig. 7. The thermal accommodation coefficient of helium is significantly lower than that of air; this is attributable to the lower atomic mass, which leads to a shorter mean interaction time with the surface. This difference is consistent with previous observations reported in the literature.[1] Measurements using helium were also performed on PDDA-coated and silanized spheres, and the results are included in Table II.

Similarly, the thermal accommodation coefficient of nitrogen on bare fused silica is found to be 0.796 ± 0.011. The value is somewhat different from that obtained for ambient air on fused silica. The difference may reflect some systematic errors that are not accounted for in our procedure, such as an offset in the pressure measurement.

TABLE II. Summary of measurements of thermal accommodation coefficient α, of various gases on different surfaces, using a fused-silica microsphere of effective radius a as the substrate.

Gas	Surface	Resonator	a (μm)	α
Air	Bare	#2	290 ± 1	0.745 ± 0.006
Air	PDDA	#3	391 ± 1	0.802 ± 0.011
Air	Silanized	#4	344 ± 1	0.767 ± 0.008
Helium	Bare	#2	299 ± 1	0.394 ± 0.003
Helium	PDDA	#3	406 ± 4	0.339 ± 0.009
Helium	Silanized	#4	356 ± 3	0.372 ± 0.009
Nitrogen	Bare	#1	429 ± 1	0.796 ± 0.011

In all experiments using the two-stem microspheres, the vacuum chamber was held at minimum pressure for a long time (~100 h) before measurements were made with increasing pressure. This ensures that the surface water coverage is reduced to less than 10% of the monolayer that is the typical atmospheric-pressure equilibrium value. Table II summarizes our results for air, helium, and nitrogen on various surfaces. The two parameters determined by fitting the model to our data, the effective radius, a, and the accommodation coefficient, α, are listed for each case. The variation in effective radius with gas may be seen by noting which microresonator was used for each entry in Table II. The larger effective radius for a given resonator when used in He may be related to the fact that the temperature-jump distance g is about three times larger for He than for air.

V. CONCLUSIONS

In conclusion, a novel method is presented for measuring thermal accommodation coefficients of various gases on a wide range of surfaces. The temperature sensitivity of the resonant frequencies of WGMs in a microsphere has been employed to measure the thermal conductivity of the ambient gas as a function of pressure. Measuring the thermal relaxation time to determine k_{gas} vs. p, and fitting the results to the temperature-jump model of Eq. (10), determines the value of the thermal accommodation coefficient of the gas on the microsphere surface, coated or uncoated. Our measurements were made at room temperature but the method is not limited to temperatures near room temperature. Since these measurements can easily be done with diverse gases, using different surface coatings (there is a lot of flexibility in choosing coating materials, as long as the deposited film is thin compared to the wavelength), a large variety of gas-surface interactions can be studied. The precision of these measurements is quite good (~1%), so the prospect of using this technique for more extensive thin-film characterization in the presence of various gases is promising. This method can also give valuable information about contaminants present on the surface and can be applied to other surface chemistry studies. This optical

technique using microresonators is very flexible and well suited to making these measurements and so adds a new method for the study of thermal transport processes involving the interaction of gases with surfaces.

ACKNOWLEDGMENTS

Sarah Bates and Seth Koterba contributed to the initial experiments investigating these effects. The vacuum chamber was constructed by Mike Lucas of the Physics/Chemistry Instrument Shop. This work has been supported by the National Science Foundation (NSF) under Grant Number ECCS-0601362 and by the Oklahoma Center for the Advancement of Science and Technology under Grant Number AR072–066.

[1]S. C. Saxena and R. K. Joshi, *Thermal Accommodation and Adsorption Coefficients of Gases*, McGraw-Hill/CINDAS Data Series on Material Properties Vol. II, edited by Y. S. Touloukian and C. Y. Ho (McGraw-Hill, New York, 1981).
[2]F. O. Goodman, J. Phys. Chem. **84**, 1431 (1980).
[3]R. E. Harris, J. Chem. Phys. **46**, 3217 (1967).
[4]W. M. Trott, J. N. Castañeda, J. R. Torczynski, M. A. Gallis, and D. J. Rader, Rev. Sci. Instrum. **82**, 035120 (2011).
[5]J. W. Lu, W. A. Alexander, and J. R. Morris, Phys. Chem. Chem. Phys. **12**, 12533 (2010).
[6]F. Liu, K. J. Daun, D. R. Snelling, and G. J. Smallwood, Appl. Phys. B **83**, 355 (2006).
[7]S.-A. Kuhlmann, J. Reimann, and S. Will, J. Aerosol Sci. **37**, 1696 (2006).
[8]A. T. Rosenberger, Opt. Express **15**, 12959 (2007).
[9]G. Farca, S. I. Shopova, and A. T. Rosenberger, Opt. Express **15**, 17443 (2007).
[10]S. L. Westcott, J. Zhang, R. K. Shelton, N. M. K. Bruce, S. Gupta, S. L. Keen, J. W. Tillman, L. B. Wald, B. N. Strecker, A. T. Rosenberger, R. R. Davidson, W. Chen, K. G. Donovan, and J. V. Hryniewicz, Rev. Sci. Instrum. **79**, 033106 (2008).
[11]V. S. Il'chenko and M. L. Gorodetskii, Laser Phys. **2**, 1004 (1992).
[12]L. Collot, V. Lefèvre-Seguin, M. Brune, J.-M. Raimond, and S. Haroche, Europhys. Lett. **23**, 327 (1993).
[13]T. Carmon, L. Yang, and K. J. Vahala, Opt. Express **12**, 4742 (2004).
[14]H. Rokhsari, S. M. Spillane, and K. J. Vahala, Appl. Phys. Lett. **85**, 3029 (2004).
[15]Q. Ma, T. Rossmann, and Z. Guo, Meas. Sci. Technol. **21**, 025310 (2010).
[16]A. T. Rosenberger, E. B. Dale, D. Ganta, and J. P. Rezac, Proc. SPIE **6872**, 68720U (2008).
[17]H. S. Carslaw and J. C. Jaeger, *Conduction of Heat in Solids* (Clarendon, Oxford, 1959), Chap. IX, pp. 230–254.
[18]W. R. Foss and E. J. Davis, Chem. Eng. Commun. **152–153**, 113 (1996).
[19]E. H. Kennard, *Kinetic Theory of Gases* (McGraw-Hill, New York, 1938), Chap. VIII, pp. 291–337.
[20]J. Orear, Am. J. Phys. **50**, 912 (1982).
[21]F. P. Incropera, D. P. DeWitt, T. L. Bergman, and A. S. Lavine, *Fundamentals of Heat and Mass Transfer* (Wiley, Hoboken, NJ, 2007), pp. 260–261.
[22]J. J. Mahony, Proc. R. Soc. London, Ser. A **238**, 412 (1957).
[23]I. H. Malitson, J. Opt. Soc. Am. **55**, 1205 (1965).
[24]A. Isihara, J. Chem. Phys. **18**, 1446 (1950).
[25]A. L. Rogach, D. S. Koktysh, M. Harrison, and N. A. Kotov, Chem. Mater. **12**, 1526 (2000).
[26]R. K. Iler, *The Chemistry of Silica: Solubility, Polymerization, Colloid and Surface Properties, and Biochemistry*, (Wiley, New York, 1979), Chap. VII, pp. 622–730.
[27]D. E. Leyden, *Silanes, Surfaces and Interfaces* (Gordon and Breach Science, New York, 1986), Chap. I, pp. 1–25.